Three-dimensional BEM analysis to assess delamination cracks between two transversely isotropic materials

N.O. Larrosa[1,3], J.E. Ortiz[2] and A.P. Cisilino[3]

[1] Departamento de Ingeniería Mecánica y de los Materiales, Escuela Superior de Ingenieros, Universidad de Sevilla. Av. de los Descubrimientos s/n, E-41092, Sevilla, España. (nlarrosa@us.es)

[2] Departamento de Mecánica de Medios Continuos, Escuela Superior de Ingenieros, Universidad de Sevilla. Av. de los Descubrimientos s/n, E-41092, Sevilla, España.

[3] División Soldadura y Fractomecánica, INTEMA. Facultad de Ingeniería, Universidad Nacional de Mar del Plata – CONICET, Av. Juan B. Justo 4302, B7608FDQ, Mar del Plata, Argentina. (cisilino@fi.mdp.edu.ar)

Abstract

Beyond the inherent attribute of reducing the dimensionality of the problem, the attraction of the Boundary Element Method (BEM) to deal with fracture mechanic problems is its accuracy to solve strong geometrical discontinuities. Within this context, it is presented in this paper a three-dimensional implementation of the Energy Domain Integral (EDI) for the analysis of interface cracks in transversely isotropic bimaterials. The EDI allows extending the two-dimensional *J*-integral to three dimensions by means of a domain representation naturally compatible with the BEM, in which the required stresses, strains and derivatives of displacements are evaluated using their appropriate boundary integral equations. To this end, the BEM implementation uses a set of recently introduced fundamental solutions for transversely isotropic materials. Several examples are solved in order to demonstrate the efficiency and accuracy of the implementation to solve straight and curved crack-front problems.

Keywords: three-dimensional interface cracks, transversely isotropic bimaterials, energy domain integral, boundary element method.

1 Introduction

High performance composite materials possess excellent mechanical properties such as strength, toughness and fatigue resistance. Composite materials are ideal for components which require high strength per weight and stiffness per weight ratios. By choosing an appropriate combination of reinforcement and matrix material, manufacturers can produce materials with mechanical properties that fit the requirements for a particular purpose. Commonly, high strength and stiffness are required in various directions within a plane.

A solution is to stack and weld together a number of plies, each having the fibres oriented in different directions. Such a stack is termed a laminate. The individual plies present a macroscopic transversely isotropic behaviour with the symmetry axis in the direction of the fibres (Gibson, 2007).

However, the application of composite materials in critical components has lagged behind due to the lack of sufficient knowledge about composite damage tolerance properties. Delamination, for example, is one of the areas that still demands a lot of work. Delamination consists in the nucleation of interface cracks between the plies of the laminate as a consequence of thermo-mechanical fatigue, impact or material degradation (Gibson, 2007). Progress in the mechanics of interface fracture has been generally focused in the two-dimensional idealization of an interface crack, and not until recently major effort has been conducted on the three-dimensional aspect of interface fracture. That is in part due to the complexity of such problems and the very large computational efforts required for their numerical analysis. However, given the material mismatch at the interface boundary, it is expected that the three-dimensional effects play a more significant role in a laminate structure than in a homogenous structure.

The numerical analysis of interface cracks in transversally isotropic materials has been traditionally addressed using Finite Element Analysis (FEA) see, for example, Boniface and Banks-Sills (2002) and Freed and Banks-Sills (2005). Besides, there is the alternative of using the Boundary Element Method (BEM). The attraction of the BEM can be largely attributed to the reduction in the dimensionality of the problem; this means that, compared to finite-element domain-type analysis, a BEM analysis results in a substantial reduction in data preparation. At the same time, and due to the inherent characteristics of its formulation, the BEM provides very accurate results for problems containing strong geometrical discontinuities. Fracture mechanical analysis of three dimensional transversely isotropic materials using BEM has been reported by Sáez et al. (1997) and Ariza and Dominguez (2004a, 2004b) who modelled static and dynamic crack problems, Zhao et al. (2007) who derived the displacement discontinuity boundary integral equation, and more recently by Chen et al. (2009) who studied the stress intensity factors of a central square crack in a transversely isotropic cuboid with arbitrary material orientations. To our knowledge, there is no published material about the three dimensional BEM modelling of interface cracks in dissimilar transversely isotropic bimaterials.

A number of techniques have been proposed for the evaluation of fracture parameters of interface cracks using FEM and BEM. They are, among others, the virtual crack extension approach (So, Lau and Ng; 2004), contour and domain path-independent integrals (Chow and Atluri, 1998; Ortiz and Cisilino, 2005; Freed and Banks-Sills, 2005; Shah, Tan and Wang, 2006), displacement extrapolation techniques (Freed and Banks-Sills, 2005; Tan and Gao, 1990; Mao and Sun, 1995) and special crack-tip elements (He, Lin and Ding, 1994). In particular, path-independent integral techniques are derived from the *J*-integral proposed by Rice

(1968). Being an energy approach, path-independent integrals eliminate the need to solve local crack tip fields accurately. If the integration domain is defined over a relatively large portion of the mesh, an accurate modelling of the crack tip is unnecessary because the crack tip field contribution to the overall energy is not significant. At the same time, it is worth noting that the *J*-integral approach developed by Rice (1968) characterizes the crack driving force for two-dimensional problems. Therefore, for general three-dimensional cases involving cracks of arbitrary shape an alternative form for the *J*-integral is needed.

Three basic schemes have evolved for the numerical computation of the *J*-integral in three dimensions: virtual crack extension methods, generalization of Rice's contour integral, and domain integral methods (Anderson, 1994). Domain integrals are equivalent to the virtual crack extension technique and are better suited for numerical analysis than contour integral methods. Among the available domain integral methods (see for example, Nikishkov and Atluri, 1987 and Saliva et al, 2000), the Energy Domain Integral (EDI) due to Moran and Shih (1987) was chosen for this work.

The EDI can be formulated by applying the divergence theorem to Rice's *J*-integral. It produces a domain independent integral defined over finite volumes enclosing some portion of the crack front (Moran and Shih, 1987). Previous works by the authors of this paper have demonstrated the versatility and efficiency of the BEM implementation of the EDI for assessing three-dimensional cracks in elastic (Cisilino et al, 1998), elastoplastic (Cisilino and Aliabadi, 1999) and thermoelastic bodies (Balderrama et al, 2006 and 2008) and for interface cracks in dissimilar isotropic bimaterials (Ortiz and Cisilino, 2005).

This work introduces the BEM implementation of the EDI for the computation of the *J*-integral in three-dimensional interface cracks in transversely isotropic bimaterials. The BEM implementation uses the fundamental solutions recently introduced by Távara et al (2008). The BEM solution strategy for the fracture problem and the EDI implementation is an extension of that proposed by Ortiz and Cisilino (2005) for interface cracks in dissimilar isotropic bimaterials. Several examples are solved and the results compared to those available in the literature.

2 Transversely isotropic materials

The basic constitutive expressions governing the elastic behaviour of transversely isotropic materials are reviewed next following Ting (1996). The general constitutive law of the anisotropic material is

$$\sigma_{ij}(x) = \mathrm{C}_{ijkl}(x)\varepsilon_{kl}(x) = \mathrm{C}_{ijkl}(x)u_{k,l}(x) \tag{1}$$

where, relative to a fixed rectangular Cartesian coordinate system, $\sigma_{ij}(x)$ are the components of the stress tensor, $\varepsilon_{ij}(x)$ are the components of the infinitesimal strain tensor and $u_k(x)$ are the components of the displacement vector. Partial derivatives are indicated using the comma notation. Also, $C_{ijkl}(x)$ are the

components of the fourth-order constitutive tensor C, that is defined in terms of 21 independent elasticity constants.

Transversely isotropic materials are those with an axis of symmetry such that all directions perpendicular to that axis are on a plane of isotropy. In such a case the constitutive tensor can be defined in terms of 5 independent elasticity constants only. Using the Voigt reduced notation, the fourth-order constitutive tensor C_{ij} $(i,j = 1,\dots,6)$ for a transversely isotropic material with the axis of symmetry coincident with the Cartesian axis x_3 can be expressed in terms of the following five elastic constants:

$$C_{1111} = C_{11},\ C_{3333} = C_{33},\ C_{1122} = C_{12},\ C_{1133} = C_{13} \text{ and } C_{2323} = C_{44}\,. \tag{2}$$

Due to the symmetry with respect to x_3, $C_{66} = (C_{11} - C_{12})/2$.

The coefficients of the constitutive tensor C_{ij} can be written in terms of the elastic engineering constants as follows:

$$C_{11} = \frac{E(n - v'^2)}{\lambda(1+v)},\ C_{12} = \frac{E(n + v'^2)}{\lambda(1+v)}, C_{13} = \frac{Ev'}{\lambda},\ C_{33} = \frac{E(1+v)}{\lambda}, C_{44} = \mu', \tag{3}$$

where

$$\lambda = n(1-v) - 2v'^2 \text{ and } n = E/E', \tag{4}$$

and

- E and E' are the Young's moduli in the plane of isotropy and in the direction normal to it, respectively.
- v is the Poisson's ratio that represents the strain response in the plane of isotropy due to an action parallel to it; and v' is the lateral strain response for the planes normal to the plane of isotropy.
- μ' is the shear modulus for the planes normal to the planes of transverse isotropy.

3 The Energy Domain Integral

Consider a three-dimensional crack front with a continuously turning tangent as depicted in Figure 1*a* with a local coordinate system x^* at position η, given by x_1^* normal to the crack front, x_2^* normal to the crack plane, and x_3^* tangent to the crack front. In addition, a tubular domain V surrounds the crack segment L_c which contains the position η.

Following Natha and Moran (1993), the *J*-integral at the position η can be computed using the Energy Domain Integral (EDI) as follows

$$J(\eta) = \frac{\bar{G}(\eta)}{\int_{L_c} \Delta a(\eta) dl}, \tag{5}$$

where $\bar{G}(\eta)$ gives the total energy released when the finite segment L_c undergoes the virtual displacement,

$\Delta a(\eta)$, in the plane of the crack (see Figure 1*b*).

The expression of the energy release rate is

$$\bar{G}(\eta) = \int_V \left(\sigma_{ij}^* u_{j,k}^* - w \cdot \delta_{ki}\right) q_{k,i} dV, \tag{6}$$

where, w is the strain energy density, σ_{ij}^* and $u_{j,k}^*$ are Cartesian components of stress and displacement derivatives expressed in the system x^*, the integration domain V is the volume of the tubular domain that surrounds the crack segment L_c, and q is an auxiliary vector function used to represent the virtual crack advance as follows (see Figure 1*b*):

$$q_k = \begin{cases} \Delta a(\eta) \cdot \xi_k(\eta) \text{ on } L_c \\ 0 \text{ on } S \end{cases} \tag{7}$$

The function q has to be smooth in V, it possess a maximum at the position η and it vanishes on the surfaces of V. The symbol $\xi_k(\eta)$ in Equation (7) stands for the k^{th} component of the unit outward normal to the crack front in the crack plane $x_1^* - x_3^*$.

Analogously to the path-independency of its classical two-dimensional counterpart, the EDI formulation of the *J*-integral is independent of the integration volume V (Natha and Moran, 1993).

4 Boundary Element Formulation and Implementation

In order to account for the non homogeneous material properties, a multi-domain BEM formulation is used for the problem solution. The modelling strategy is illustrated in the schematic representation in Figure 2 for a model consisting of two subdomains, $\Omega_I(x)$ and $\Omega_{II}(x)$, with external boundaries $\Gamma_I(x)$ and $\Gamma_{II}(x)$, respectively. Both subdomains share a common interface $\Gamma_{I-II}(x)$, a portion of which is debonded and thus an interface crack is introduced. The subdomains possess linear transversely isotropic material behaviours as described in Section 2. The orientation of the material is specified using a local Cartesian system (x_1^0, x_2^0, x_3^0) for each subdomain. In every case the direction of the symmetry axis of the material is chosen coincident with the direction x_3^0 (see Figure 2). In this way, it is possible to model interface cracks lying between laminates with arbitrary relative orientations.

The standard BEM uses the displacement boundary integral equation to relate the displacement and traction fields, $u(x)$ and $t(x)$ over the model boundary in the global coordinate system (see Aliabadi, 2002):

$$c_{ik}(x')u_i(x') + \int_\Gamma T_{ik}(x, x')u_i(x)\mathrm{d}\Gamma(x) = \int_\Gamma U_{ik}(x, x')t_i(x)\mathrm{d}\Gamma(x), \tag{8}$$

where $U_{ik}(x, x')$ and $T_{ik}(x, x')$ are the displacement and traction fundamental solutions for transversely isotropic materials, respectively. The fundamental solutions account for the solution of *i-th* component of the

displacement and traction fields, $u_i(x)$ and $t_i(x)$, at the field point, x, due to the action of a unit load acting in the direction j at the source point, x' (see next section for the details about the fundamental solutions used in this work). The symbol c_{ik} is the so-called jump term which depends on the local geometry at the source point, x', only.

BEM models are discretized using 9-node quadrilateral elements. Continuous elements are used everywhere in the model, except at the intersections of the interface and the crack faces with model outer surface. In such cases one- and two-side discontinuous elements are used in order to avoid common nodes at the intersections (see Figure 3). It is worth noting that, although discontinuous elements are not strictly necessary to solve most of the practical bimaterial crack problems, they have been implemented in this work in order to develop a versatile and robust discretization strategy capable of dealing with general multiple subdomain problems (including the case of more than two subdomains sharing a single edge). At the same time, the implementation remains open to introduce further extensions to account for crack propagation which could require automatic model remeshing.

The regular BEM integrals over continuous and discontinuous elements are evaluated using standard Gaussian quadrature. In the case of nearly singular integrals an adaptive element subdivision technique is also employed. On the other hand, the Cauchy principal value integrals and the free terms are evaluated using the rigid body motion approach (see Aliabadi, 2002). Singular integrals are computed using the variable transformation technique due to Lachat and Watson (1976).

The equilibrium and continuity conditions are enforced at the nodes lying on the interface Γ_{I-II} shared by the two regions. In the case that no external forces are applied on the interface, the equilibrium condition is $t_I = -t_{II}$. The continuity condition is $u_I = u_{II}$. For further details on the multi-domain BEM formulation and implementation the reader is referred to the book by Aliabadi (2002).

Comninou (1977) showed that the solution of the stress fields for a crack between dissimilar materials always predict a contact zone between the crack surfaces at the crack tip. However, according to Rice (1988) elastic fracture mechanics procedures are still valid when the inevitable non-linear contact zone size is small compared with the crack size. It is assumed in this work that this condition is always satisfied, and so, the BEM implementation does not account for contact between the crack surfaces.

The computation of the *J*-integral is included in the BEM code as a post-processing procedure, and so, it could be applied to the results from a particular model at a later stage. The required stresses, strains and derivatives of displacements at internal points are directly obtained from their boundary integral representations (Aliabadi, 2002):

$$u_{i,m}(X') = \int_\Gamma U_{ij,m}(x, X') t_j(x) \mathrm{d}\Gamma(x) - \int_\Gamma T_{ij,m}(x, X') u_j(x) \mathrm{d}\Gamma(x) \tag{9}$$

where X' is the coordinate of the internal point, $U_{ij,m}(x,X')$ and $T_{ij,m}(x,X')$ are the derivatives of the fundamental displacement and traction fundamental solutions. The boundary Γ corresponds to the boundary of the subdomain where the internal point X' lies on. Strains and stresses at internal points can then be easily computed using the definition of the infinitesimal strain tensor $\varepsilon_{ij} = \left(u_{i,j} + u_{j,i}\right)/2$ and the constitutive relations in equation (1).

On the other hand, the derivatives of the displacements, strains and displacements for boundary points are evaluated from the boundary displacements and tractions by means of a procedure similar to that usually used for finite elements. For further details the reader is referred to the paper by Ortiz and Cisilino (2005).

Finally, and in order to proceed with the *J*-integral computation, the resultant displacement derivatives, strains and stresses for both internal and boundary points are transformed to the local crack-front coordinate system (x_1^*, x_2^*, x_3^*) introduced in Section 3 using the standard transformation rule for second-order tensors (see Ting, 1996).

5 The Fundamental Solutions for Transversely Isotropic Materials

There are several expressions for the fundamental solutions for a transversely isotropic materials; see, for example, Pan and Chou (1976) and Loloi (2000). However, these solutions could be cumbersome to implement into a BEM code because of the multiple cases to consider due to all possible material orientations and the relative positions of the source and field points.

Távara et al. (2008) have recently derived completely general and unique expressions valid for all possible configurations given in terms of real functions only. These fundamental solutions are presented in what follows.

The Green's function for linearly elastic anisotropic medium using the Barnett-Lothe tensor is (Lifshitz and Rozentsveig, 1947)

$$U^0(x) = \frac{1}{4\pi r} H(x), \tag{10}$$

where *x* is the position vector and the matrix $H(x)$ defined by

$$H(x) = \frac{1}{\pi}\int_{-\infty}^{+\infty} \Gamma^{-1}(p)dp. \tag{11}$$

The integrand $\Gamma(p)$ is the 3×3 matrix

$$\Gamma(p) = Q + p(R + R^T) + p^2 T \tag{12}$$

where the super-index *T* means the transpose of the matrix. The matrices *Q*, *R* and *T* are defined as follows

$$Q_{ij} = C_{ijks} n_j n_s, \;\; R_{ik} = C_{ijks} n_j m_s, \;\; T_{ik} = C_{ijks} m_j m_s \,, \tag{13}$$

where n and m are orthogonal unit vectors in the plane normal to the position vector x. The matrices Q and T are symmetric and positive definite if the deformation energy of the material is positive. Considering (12) and (13), the matrix $H(x)$ is also symmetric and it depends of the direction of the position vector x, but not on its magnitude. Using the residues theory, $H(x)$ in equation (11) can be expressed in the same form of equations (10) and (12):

$$H(x) = 2i \sum_{v=1}^{3} \frac{\hat{\Gamma}(p_v)}{|\Gamma(p)|'}, \tag{14}$$

where $\hat{\Gamma}(p_v)$ is the adjunct of the matrix of $\Gamma(p)$ defined in equation (12) and $|\Gamma(p)|$ is its determinant. The values p_v are the so-called Stroh eigenvalues of the sextic equation:

$$|\Gamma(p)| = 0. \tag{15}$$

The eigenvalues of equation (15) can be represented as $p_v = \alpha_v + i\beta_v$ where both α_v and β_v are real with $\beta_v > 0$ (v=1,2,3). Although there are explicit solutions for equation (14) in terms of the eigenvalues, p_v, and for Green's function in equation (10), they are not of practical use here because they are not general and they do not hold for the degenerate cases $p_1 = p_2$ and $p_1 = p_2 = p_3$. Alternatively, a simplified solution for equation (14) can be obtained when equation (15) is a cubic equation in p^2 of the form

$$|\Gamma(p)| = |T|(p^2 - p_1^2)(p^2 - p_2^2)(p^2 - p_3^2)\,. \tag{16}$$

In this case, equation (15) can be expressed as

$$[p^4 + (g^2 - 2h)p^2 + h^2)][p^2 + \beta_3^2] = 0. \tag{17}$$

where g, h and β_3 are defined in Appendix A.

A new expression for $H(x)$ is obtained for any anisotropic linear elastic material

$$H(\mathrm{x}) = \frac{1}{|\mathrm{T}|} \sum_{n=0}^{4} p^n \hat{\Gamma}^{(n)}\,. \tag{18}$$

Using equations (16) and (18) with (14), the following expression results

$$H(\mathrm{x}) = \frac{1}{|\mathbf{T}|\xi} \left\{ \frac{\zeta}{h\beta_3} \hat{\Gamma}^{(0)} + \hat{\Gamma}^{(2)} + \delta \hat{\Gamma}^{(4)} \right\} \tag{19}$$

where

$$\zeta = -i(p_1 + p_2 + p_3) = g + \beta_3 \tag{20}$$

$$\delta = -(p_1 p_2 + p_2 p_3 + p_3 p_1) = h + g\beta_3 \tag{21}$$

$$\xi = i(p_1 + p_2)(p_2 + p_3)(p_1 + p_3) = g(h + g\beta_3 + \beta_3^2). \tag{22}$$

The terms ζ, δ and ξ depend only on $p_1 + p_2$, $p_1 p_2$ and p_3; therefore, it is not necessary to calculate all the eigenvalues. It is worth noting that the solution to equation (19) is valid for degenerate and non-degenerate cases. The terms β_3, h and g can be computed using equation (17).

A relatively simple and general expression for $H(x)$ for transversely isotropic materials can be obtained using the auxiliary vector $\hat{x} = (r_{12}, 0, x_3^0)$, where $r_{12} = [(x_1^0)^2 + (x_2^0)^2]^{1/2}$, (x_1^0, x_2^0, x_3^0) is the local coordinate system, and the triad $[n, m, \hat{x}/r]$ with $n = (c, 0, -s)$ and $m = (0, 1, 0)$ where $c = cos\,\phi = x_3^0/r$

and $s = sin\ \phi = r_{12}/r$, and $0 \leq \phi \leq \pi$, is illustrated in Figure 4. For such a coordinate system, the only non-zero coefficients are given by

$$H_{11} = \frac{1}{\mathrm{C}_{66}\beta_3} + \frac{\mathrm{C}_{44}c^2 + \mathrm{C}_{33}s^2}{\mathrm{C}_{11}\mathrm{C}_{44}gh} - \frac{f}{\xi} \tag{23}$$

$$H_{22} = \frac{1}{\mathrm{C}_{11}g} + \frac{f}{\xi} \tag{24}$$

$$H_{33} = \frac{1}{gh}\left\{\frac{h + c^2}{\mathrm{C}_{44}} + \frac{s^2}{\mathrm{C}_{11}}\right\} \tag{25}$$

$$H_{13} = \frac{(\mathrm{C}_{13} + \mathrm{C}_{44})sc}{\mathrm{C}_{11}\mathrm{C}_{44}gh} \tag{26}$$

The additional terms in equations (23), (24), (25) and (26) are given in Appendix A. The general expression of the tensor $H(x)$ for any *x* can be obtained by transformation of components:

$$H_{ij}(x) = \Omega_{ik}\ \Omega_{\mathrm{js}} H_{ks}(\hat{x}), \tag{27}$$

where the rotation matrix Ω_{ij} is

$$\Omega_{\mathrm{ij}} = \begin{pmatrix} \cos\theta & -\sin\theta & 0 \\ \sin\theta & \cos\theta & 0 \\ 0 & 0 & 1 \end{pmatrix}. \tag{28}$$

The derivatives of the displacement fundamental solution can be expressed using the modulation function $\widehat{U}_{ij,k}(x)$:

$$U^0_{ij,k}(x) = \frac{\widehat{U}_{ij,k}(x)}{4\pi r^2}. \tag{29}$$

$\widehat{U}_{ij,k}(x)$ is an odd function, which depends on the direction of *x*, but not on its magnitude, i.e. $\widehat{U}_{ij,k}(x) = -\widehat{U}_{ij,k}(-x/r)$. Using the transformation in (27), the derivatives of the displacement fundamental solution are:

$$\widehat{U}_{ij,k}(x) = \Omega_{ia}\Omega_{jb}\Omega_{kc}\widehat{\mathrm{U}}_{ab,c}(\hat{x})\ . \tag{30}$$

The closed-form expressions of $\widehat{U}_{ij,k}(\hat{x})$ can be found in Távara et al (2008).

Besides, the stresses fundamental solution, $\Sigma_{ijk}(x)$, can be obtained by applying the Hooke's law for transversely isotropic material, yielding

$$\Sigma^0_{ijk}(x) = \frac{\hat{\Sigma}_{ijk}(x)}{4\pi r^2}, \tag{31}$$

where $\hat{\Sigma}_{ijk}(x)$ is an odd symmetric function. So, the stress fundamental solution can be expressed in a similar form to equation (30):

$$\hat{\Sigma}_{ijk}(x) = \Omega_{ia}\Omega_{\mathrm{jb}}\Omega_{\mathrm{kc}}\hat{\Sigma}_{abc}(\hat{x}). \tag{32}$$

The closed-form expressions of $\hat{\Sigma}_{ijk}(\hat{x})$ can be found in Távara et al (2008). The traction fundamental solution associated to the normal vector $n_j(x)$ can be obtained directly using:

$$T_{ik}^{o}(x) = \Sigma_{ijk}^{0}(x) n_j(x). \tag{33}$$

Finally, the fundamental solutions $U_{ik}(x)$ and $T_{ik}(x)$ have to be transformed from the local coordinate system, (x_1^0, x_2^0, x_3^0), to the global one in order to assemble the boundary integral equation (8). The fundamental solutions are transformed from the local coordinate system to the global one via the standard transformations for second order tensors (see Ting, 1996):

$$U_{ij}(x) = a_{ik} a_{jl} U_{kl}^{o}(x),\ T_{ij}(x) = a_{ik} a_{jl} T_{kl}^{o}(x), \tag{34}$$

where a_{ik} are the coefficients of the transformation matrix.

6 *J*-integral Computation

The computation of the EDI was included in the BEM code as a post-processing procedure, and so it could be applied to the results from a particular model at a later stage. As it has been stated in Section 3, equation (5) allows the computation of the *J*-integral at any position $\boldsymbol{\eta}$ on the crack front. In each case, this requires the evaluation of a volume integral over a domain that enclose a segment of the crack front, $\boldsymbol{L_c}$. A natural choice here is to make $\boldsymbol{\eta}$ coincident with the element nodes on the crack front, while $\boldsymbol{L_c}$ is taken as the element or element sides at which the point $\boldsymbol{\eta}$ lies. As it is depicted in Figure 5, three different cases are considered depending on whether the node *M* at the location of the crack front position $\boldsymbol{\eta}$ is a mid-side node, it is shared by two elements, or it is located coincident with the external surface (surface node). If the node *M* is a mid-side node or surface node, $\boldsymbol{L_c}$ (the width of the integration domain) spans over one element, connecting nodes *M*-1, *M*, and *M*+1 and nodes *M*-2, *M*-1 and *M*, respectively. On the other hand, if the node *M* is a shared by two elements, $\boldsymbol{L_c}$ spans over the two elements, connecting nodes from *M*-2 to *M*+2.

The boundary mesh is designed to have a web pattern around the crack front in order to build the integration domains for the evaluation of the EDI with the shape of cylinders. The integration volumes are discretized using 27-noded isoparametric (brick) cells. This is illustrated in Figure 6, where a portion of the model surface has been removed to show the discretizations of the crack and of the integration domains.

Stresses, strains and derivatives of displacements at cell nodes are computed using the procedures introduced in Section 4, and then transformed to the local the crack-front coordinate system, $(\boldsymbol{x_1^*}, \boldsymbol{x_2^*}, \boldsymbol{x_3^*})$, using the standard transformation rule for second-order tensors. The stresses, strains and displacements derivatives are approximated within cell domains by products of the cell interpolation functions, $\boldsymbol{\Psi_i}$, and the nodal values of $\boldsymbol{\sigma_{ij}^*}$, $\boldsymbol{\varepsilon_{ij}^*}$ and $\boldsymbol{u_{i,m}^*}$.

A central point in the implementation of the EDI is the specification of the values for the function $\boldsymbol{q}$. Following the definition introduced in equation 7, the value of $\boldsymbol{q_k}$ is specified equal to one for the cell node coincident with the position $\boldsymbol{\eta}$ on the crack front where the EDI is evaluated, and equal to zero for all the cell nodes located on the surface of the integration volume. For the implementation used in this work, the function $\boldsymbol{q}$ is chosen to vary quadratically in the directions tangential and normal to the crack front (this is schematically illustrated in Figure 5 for the tangential direction on the plane plane $(\boldsymbol{x_1^*}, \boldsymbol{x_3^*})$). This bi-quadratic definition of $\boldsymbol{q}$ has been employed with excellent results in the computation of EDI for a variety of

problems in previous works (see Cisilino et al, 1998; Cisilino and Aliabadi, 1999; Ortiz and Cisilino, 2005 and Balderrama et al., 2006 and 2008). Thus, considering that the evaluation point $\boldsymbol{\eta}$ is at the middle of the crack front segment, $\boldsymbol{L_c}$, and $\boldsymbol{r_0}$ is the radius of the integration domain, the function $\boldsymbol{q}$ is written as:

$$q(x^*) = \left| 1 - \left(\frac{x_3^*}{\frac{L_c}{2}} \right)^2 \right| \cdot \left[1 - \left(\frac{r}{r_0} \right)^2 \right] \tag{35}$$

where $\boldsymbol{r}$ is the distance from the crack front in the $\boldsymbol{x_1^* - x_2^*}$ plane (see Figure 1).

Equation (35) is used to specify the value of $\boldsymbol{q}$ for all the cell nodes within the integration domain. Then, consistent with the isoparametric formulation, the *q*-values are interpolated within each volume cell using

$$q = \sum_{i=1}^{27} \Psi_i Q^i, \tag{36}$$

where $\boldsymbol{\Psi_i}$ are the shape functions and $\boldsymbol{Q^i}$ is the *q*-value for the *i*th node. Following standard manipulations, the derivatives of $\boldsymbol{q}$ are:

$$q_{k,j} = \sum_{i=1}^{27} \sum_{l=1}^{3} \frac{\partial \Psi_i}{\partial \zeta_l} \frac{\partial \zeta_l}{\partial x_j^*} Q^i, \tag{37}$$

where $\boldsymbol{\zeta_k}$ are the coordinates in the cell isoparametric space and $\boldsymbol{\partial \zeta_k / \partial x_j^*}$ is the Jacobian matrix of the transformation.

Finally, if Gaussian integration is used, the discretized form of expression (6) is

$$\bar{G}(\eta) = \sum_{\text{cells in } V} \sum_{p=1}^{m} \left\{ \left(\sigma_{ij}^* u_{j,k}^* - \sigma_{ij}^* \varepsilon_{ij}^* \delta_{ki} \right) q_{k,j} det \left(\frac{\partial x_j}{\partial \zeta_k} \right) \right\}_p w_p, \tag{38}$$

where $\boldsymbol{m}$ is the number of Gaussian points per cell, and $\boldsymbol{w_p}$ are their weighting factors.

7 Application Examples

7.1 Thick bimaterial plate in tension with a centre interface crack

A thick bimaterial plate containing a through crack on the interface is considered in the first example. A schematic representation of the problem geometry, dimensions and boundary conditions are depicted in Figure 7. Model discretization is similar to that depicted in Figure 6. It consists of 658 elements and 2855 nodes. Eighteen elements are placed along the crack front and a total of 126 elements are used in the crack discretization. Five rings of cells with normalized radii r/a = 0.1, 0.2, 0.3, 0.44 and 0.64 are used around the crack front for *J* computations. With this purpose 648 cells and 6438 nodes are employed.

In order to validate the code, the problem was solved first for homogeneous cases, that is, the material elastic constants and orientations were set the same for both subdomains. Thus, the direction of the axis of symmetry, $\boldsymbol{x_3^0}$, was chosen to be parallel to the crack plane, that is, coincident with the global directions *x* and *z*, respectively. The material elastic constants were chosen the same to those of the laminated used by Ariza and Dominguez (2004b). The five independent values of the elastic constants $\boldsymbol{C_{ij}}$ in expression (3) are

$$C_{11} = 5.37 \text{ GPa},\ C_{12} = 1.34 \text{ GPa},\ C_{13} = 3.35 \text{ GPa},\ C_{33} = 251.168 \text{ GPa},\ \text{and } C_{44} = 5 \text{ GPa}. \quad (39)$$

The associated elastic properties are: E= 5 GPa, E'= 247.83 GPa, ν=0.245, ν'= 0.01 and μ'= 2.5. The material orientation is specified for each subdomain by means of the angles which define the orientation of the material axis of symmetry, $\boldsymbol{x_3^0}$, with respect to the global coordinate system $(\boldsymbol{x, y, z})$. In this way, for the material axis of symmetry oriented in the global direction x, the orientation angles are 0°/90°/90°, while for the material axis of symmetry oriented in the global direction z, the angles are 90°/90°/0°.

Computed results along the crack front are presented in Figure 8. In order to compare with other results, data in Figure 8 is presented in terms of normalized stress intensity factors (SIF), $\boldsymbol{K_I/K_0}$, where $\boldsymbol{K_0 = \sigma\sqrt{\pi a}}$. To compute the stress intensity factors from the J results the expressions due to Chu and Hong (1990) are used:

$$J_1 = a_{11}K_I^2 + a_{12}K_IK_{II} + a_{22}K_{II}^2,\ \ J_2 = b_{11}K_I^2 + b_{12}K_IK_{II} + b_{22}K_{II}^2, \quad (40)$$

where the coefficients $\boldsymbol{a_{ij}}$ and $\boldsymbol{b_{ij}}$ depend on the elastic material properties and the material orientation. The coefficients $\boldsymbol{a_{12}}$, $\boldsymbol{a_{22}}$ and the three coefficients $\boldsymbol{b_{ij}}$ are zero when one of the principal axes of the material is parallel to the crack plane. Thus, for the cases considered in this work,

$$J_1 = a_{11}K_I^2. \quad (41)$$

The values for the coefficient $\boldsymbol{a_{11}}$ as a function of the ratio between the Young modulus in the xy plane, $\boldsymbol{E_x/E_y}$, are reported in Table 1.

It can be seen in Figure 8 that with the only exceptions of the regions next to the lateral faces of the specimen (say, $|\boldsymbol{z/t}| > 0.45$) where the boundary layer effect takes place, the stress intensity factor value is nearly constant along the crack front. Two sets of results obtained from a two-dimensional high-resolution finite element model are also shown in Figure 8. The finite element model was solved using Abaqus (2009), and it was discretized using a fine regular mesh consisting of 9,600 8-node biquadratic, plane stress elements (CPS8R). The stress intensity factors were computed using the Abaqus built-in J-integral procedure. The resultant normalized stress intensity factors are $\boldsymbol{K_I/K_0 = 1.124}$ and $\boldsymbol{K_I/K_0 = 1.184}$ for the material axis of symmetry oriented in the global directions x and z, respectively. The maximum difference between the BEM and FEM results along the crack front in the interior of the specimen (that is, excluding the the regions next to the lateral faces) is less than 2%.

The final case consists in a heterogeneous plate with the axis of symmetry of the material oriented in the global directions z and y for the subdomains I and II, respectively; that is, 90°/90°/0° for the subdomain I and 90°/0°/90° for the subdomain II. The material elastic properties are the same of the previous cases. Computed results are presented in Table 2. The results are normalized with respect to $\boldsymbol{J_0 = \sigma^2\pi a/E'}$. It can be seen that the J value is nearly constant along the complete crack front. Besides, the path independence is found excellent with a standard deviation of around 5% for the results computed using the domains with radii $\boldsymbol{r/a \geq 0.20}$. The only exceptions are the positions next to the lateral face of the specimen, where the boundary layer effect takes place and the applicability of the J-integral is not strictly valid. The smallest integration domains with $\boldsymbol{r/a = 0.10}$ do not provide accurate results. That is attributed to the fact that these

domains are discretized using a single cell in the radial direction. Similar behaviours were found in previous works by the authors (see, for example, Cisilino et al., 1998 and Ortiz and Cisilino, 2005).

7.2 Bimaterial laminate with an edge interface crack

It is considered in this example the analysis of an edge crack in a bimaterial laminate. The model geometry and discretization are shown in Figure 9. Model dimensions are crack length a=10 mm, specimen width b=4a, height h=a and thickness $2t$=1.5a. Material properties are the same ones used in the previous example. The discretization consisted of 596 elements. Five rings of cells with normalized radii r/a = 0.05, 0.1, 0.15, 0.22 and 0.32 are used around the crack front for the J computations. Five hundred and four cells are used in the construction of the integration domains.

The model was solved for a number of relative orientations of the axis of symmetry of the material in both subdomains. The computed results are reported in Figure 10. J-results in Figure 10 are normalized with respect to $\boldsymbol{J_0 = \sigma^2 \pi a / E'}$. It can be seen that when one of the principal axes of the material is specified perpendicular to the crack front direction for both subdomains, the J-integral results along the crack front are symmetric with respect to the specimen mid-plane (z/t=0). These are the cases for the results labelled 90°/90°/0°-90°/90°/0° and 0°/90°/90°-90°/90°/0° in the figure. On the other hand, when there is not a principal axes of the material oriented perpendicular to the crack front in at least one of the subdomains, the J-integral results are not symmetric with respect to the specimen mid-plane. The extreme values for the J-integral are attained at the free surface.

7.3 A circumferential interface crack in a cylindrical bimaterial bar

The last example consists in a cylindrical bimaterial bar containing a circumferential crack subjected to remote axial tension σ, as illustrated in Figure 11a. The radius of the bar is b=5a and its height h=24a, being a the crack depth. A total of 684 elements are employed in the model discretization. Four rings of cells with radii r/a = 0.25, 0.5, 0.75 and 1 are used around the crack front for the J computations. Integration domains are constructed using 672 cells. The model discretization is illustrated in Figure 11b. Material properties are the same reported for the previous examples.

The problem was solved considering different material orientations. The results are shown in Figure 12. In every case the results are normalized with respect to $\boldsymbol{J_0 = \sigma^2 \pi a / E'}$. The first solution is for an isotropic homogeneous material and it was used with validation purposes. The J result is constant along the complete crack front. Also plotted in Figure 12 is the result by Murakami and Okazaki (1976), which possesses a reported accuracy of 3%. The difference between the computed result and that of the reference is 5%. The second solution is for a homogeneous transversely-isotropic case, with the material symmetry axis specified coincident with the direction y for both subdomains (results labeled 90°/0°/90°-90°/0°/90° in Figure 12). Once again, and as it was expected, the computed J values are constant along the complete crack front. In the third case the orientation of the material axis of symmetry are different in each subdomain: for the subdomain I the material axis of symmetry is oriented in the z-direction, while for the subdomain II it is

oriented in the *y*-direction (results labelled 90°/90/0°-90°/0°/90° in Figure 12). The *J* results exhibit a periodic variation along the crack front. Minimum values occur in the positions coincident with the direction of the *z*-axis, while the maximum values are in the positions coincident with the direction of the *x*-axis. In the last case, the orientation of the material axis of symmetry is specified in the *x*-direction for both subdomains (results labelled 0°/90/90°-0°/90°/90° in Figure 12). As for the previous case, the *J* results exhibit a periodic variation along the crack front. However, in this case minimum values occur in the positions coincident with the direction of the *x*-axis, while the maximums are in the positions coincident with the direction of the *z*-axis.

8 Conclusions

A boundary element implementation of the EDI for the computation of the *J*-integral of three-dimensional interface cracks in transversely isotropic bimaterials has been presented in this paper. The analysis is addressed using a multidomain BEM formulation in order to account for the different material properties at both sides of the crack. The *J*-integral computation is implemented as a post-processing technique, and so, it can be applied to the results from a particular model at a later stage. The BEM uses a versatile set of fundamental solutions given in terms of real functions only which are valid for all possible material configurations. The implementation takes advantage of the efficiency of the boundary integral equation to directly obtain the required displacement derivatives, stress and strain fields from their boundary integral representations.

The efficiency and accuracy of the proposed implementation has been addressed by analysing a number of examples with straight and curved crack fronts. The computed results compared very well with those reported in the literature for benchmark problems. Besides, the implemented algorithm allowed studying the effect of the relative orientations of the materials on both sides of the crack on the *J* integral values.

Maximum errors and dependence of the computed results with the integration paths occur for surface cracks at the intersection of the crack front with a free surface. This behaviour is attributed to the boundary layer effect taking place at the intersection of the crack front and a free surface. Under these circumstances, the EDI is not strictly applicable. This problem remains unsolved in this work. Following previous work (Cisilino and Ortiz, 2005), alternative approaches for the selection of the auxiliary function $\boldsymbol{q}$ for the implementation of the EDI could be explored to improve the accuracy of the computations.

Acknowledgements

This work has been partially supported by the Agencia Nacional de Promoción Científica y Tecnológica (ANPCyT) of Argentina through the grant PICT 2007 Nº 1154. J.E. Ortiz has been supported by the Programa Ramón y Cajal of the Spanish Ministry of Science and Innovation.

References

Abaqus 6.9-1 (2009). Dassault Systemes, Providence, RI, USA.

Aliabadi M.H. (2002). *The Boundary Element Method, Volume II: Applications in Solids and Structures*. Wiley, Chichister, UK.

Anderson T.L. (2004). *Fracture Mechanics: Fundamentals and Applications*. Second Edition, CRC Press, Boca Ratón, USA.

Ariza M.P. and Dominguez J. (2004a). Dynamic BE analysis of 3-D cracks in transversely isotropic solids. *Computer Methods in Applied Mechanics and Engineering*, 193/9-11: 765-779.

Ariza M.P. and Dominguez J. (2004b). Boundary element formulation for 3D transversely isotropic cracked bodies. *International Journal for Numerical Methods in Engineering*, 60/4: 719-753.

Balderrama R., Cisilino A.P., Martinez M. (2006). BEM analysis of three-dimensional fracture problems using the energy domain integral. *ASME Journal of Applied Mechanics*, 73/6:959-969.

Balderrama R., Cisilino A.P., Martinez M. (2008). Boundary element analysis of three-dimensional mixed-mode thermoelastic crack problems using the interaction and the energy domain integrals. *International Journal for Numerical Methods in Engineering*, 74/2: 294-320.

Boniface V. and Banks-Sills L. (2002). Stress intensity factors for finite interface cracks between a special pair of transversely isotropic materials. *ASME Journal of Applied Mechanics*, 69/3: 230-239.

Chen C-S, Chen C-H and Pan E. (2009). Three-dimensional stress intensity factors of a central square crack in a transversely isotropic cuboid with arbitrary material orientations. *Engineering Analysis with Boundary Elements*, 33: 128– 136

Chow W. T. and Atluri S. N. (1998). Stress intensity factors as the fracture parameters for delamination crack growth in composite laminates. *Computational Mechanics*, 21: 1-10.

Chu S.J. and Hong C.S. (1990). Application of the J_k integral to mixed mode crack problems for anisotropic composite laminates. *Engineering Fracture Mechanics*, 35/6:1093-1103.

Cisilino A.P., Aliabadi M.H. and Otegui J.L. (1998). Energy domain integral applied to solve centre and double-edge crack problems in three dimensions. *Theoretical and Applied Fracture Mechanics*, 29:181-194.

Cisilino A.P. and Aliabadi M.H. (1999). Elastoplastic BEM implementation of the energy domain integral for the analysis of 3D fracture problems. *International Journal of Fracture*, 96:229-245.

Comninou M. (1977). The interface crack. *ASME J. Appl. Mech.*, 44: 631-636.

Freed Y. and Banks-Sills L. (2005). A through interface crack between a ±45◦ transversely isotropic pair of materials. *International Journal of Fracture* , 133: 1–41.

Gibson R.F. (2007). *Principles of Composite Material Mechanics*. CRC Press, London.

He W.J., Lin D.S. and Ding, H.J. (1994). A boundary element for crack analysis at a bimaterial interface. *Engineering Fracture Mechanics*, 49/3:405-410.

Lachat J.C. and Watson J.O. (1976). Efective numerical treatment of boundary integral equations: a formulation for three-dimensional elastostatics. *International Journal for Numerical Methods in Engineering*, 10: 991-1005.

Lifshitz I.M. and Rozentsveig L.N. (1947). Construction of the Green's tensor for the fundamental equation of elasticity theory in the case of unbounded elastically anisotropic medium. *Zh. eksper. i teoreticheskoi fiziki*, 17:783.

Loloi M. (2000). Boundary integral equation solution of three-dimensional elastostatic problems in transversely isotropic solids using closed-form displacement fundamental solutions. *International Journal for Numerical Methods in Engineering*, 48: 823-842.

Mao R. and Sun G. (1995). A study of the interaction between matrix crack and matrix-fibre interface. *Engineering Fracture Mechanics*, 51/3: 469-477.

Moran B. and Shih C.F. (1987). A general treatment of crack tip contour integrals. International *Journal of Fracture*, 35/4: 295-310.

Murakami Y. and Okazaki Y. (1976). A simple procedure for the accurate determination of stress intensity factors by finite element method. *Trans. Japan Soc. Mech. Engrs.*, 42/364: 3679-3687

Natha R. and Moran B. (1993). Domain integrals for axisymmetric interface crack problems. *International Journal of Solids & Structures*, 30/15: 2027-2040.

Nikishkov G.P. and Atluri S.N. (1987). Calculation of fracture mechanics parameters for an arbitrary three-dimensional crack by the equivalent domain integral method. *International Journal of Numerical Methods in Engineering*, 24/9:1801-1821.

Ortiz J.E. and Cisilino A.P. (2005). Boundary element method for J-integral and stress intensity factor computations in three-dimensional interface cracks. *International Journal of Fracture*, 133:197-222.

Pan Y. and Chou, T. (1976). Point solution for an infinite transversely isotropic solid. *Journal of Applied Mechanics*, 98: 608-612.

Rice J.R. (1968). A path independent integral and the approximate analysis of strain concentration by notches and cracks. *ASME Journal of Applied Mechanics*, 379-386.

Rice, J.R. (1988). Elastic fracture mechanics concepts for interracial cracks. *ASME J. Appl.Mech.*, 55: 98-103.

Sáez A., Ariza, M.P. and Dominguez J. (1997) Three-dimensional fracture analysis in transversely isotropic solids. *Engineering Analysis with Boundary Elements*, 20/4: 287-298.

Saliva R., Vénere M.J., Padra C., Taroco E. y Feijoó R.A. (2000). Shape sensitivity analysis and energy release rate of planar cracks embedded in three-dimensional bodies. *Computer Methods in Applied Mechanics and Engineering*, 188: 649-664.

Shah P.D., Tan C.L. and Wang X. (2006). Evaluation of T-stress for an interface crack between dissimilar anisotropic materials using the boundary element method. *Computer Modelling in Engineering & Science*, 13/3:185-197.

So W.M.G., Lau K.J. and Ng S.W. (2004). Determination of stress intensity factors for interfacial cracks using the virtual crack extension approach. *Computer Modeling in Engineering & Science*, 5/3:189-200.

Tan C.L. and Gao Y.L. (1990). Treatment of bimaterial interface crack problems using the boundary element method. *Engineering Fracture Mechanics*, 36: 919-932.

Távara L., Ortiz J.E., Mantic, V. and París, F. (2008). Unique real-variable expressions of displacement and traction fundamentals solutions covering all transversely isotropic elastic materials for 3D BEM. *International Journal for Numerical Methods in Engineering*, 74:776-798.

Ting T.C.T. (1996). *Anisotropic Elasticity: Theory and Applications*. Oxford University Press, Oxford, UK.

Zhao M.H., Fan C.Y. Liu T. and Yang F. (2007). Extended displacement discontinuity Green's functions for three-dimensional transversely isotropic magneto-electro-elastic media and applications. *Engineering Analysis with Boundary Elements*, 31:547-558.

Appendix A

Additional terms of the components of the tensor $H(\hat{x})$:

$$\beta_3 = \left\{\frac{\mathrm{C}_{44}c^2 + \mathrm{C}_{33}s^2}{\mathrm{C}_{66}}\right\}^{1/2}, \tag{A1}$$

$$h = \left\{c^4 + \frac{\eta s^2 c^2}{\mathrm{C}_{11}\mathrm{C}_{44}} + \frac{\mathrm{C}_{33}s^4}{\mathrm{C}_{11}}\right\}^{1/2}, \tag{A2}$$

$$g = \left\{2(h + c^2) + \frac{\eta s^2}{\mathrm{C}_{11}\mathrm{C}_{44}}\right\}^{1/2}, \tag{A3}$$

$$\xi = g(h + g\beta_3 + \beta_3^2), \tag{A4}$$

$$\eta = \mathrm{C}_{11}\mathrm{C}_{33} - \mathrm{C}_{13}^2 - 2\mathrm{C}_{13}\mathrm{C}_{44}, \tag{A5}$$

$$f = \frac{h + c^2}{C_{66}} + \frac{gh}{C_{66}\beta_3} + \frac{C_{33}s^2}{C_{11}C_{44}} \tag{A6}$$

where $= \cos\phi = x_3/r$, $s = \sin\phi = r_{12}/r$ and the angle ϕ is indicated in Figure 4.

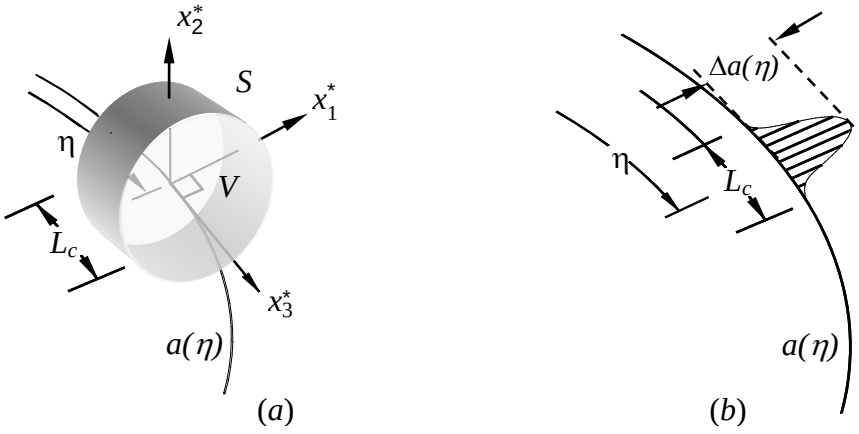

Figure 1: (*a*) Definition of the local orthogonal Cartesian coordinates at point η on the crack front and the integration volume, (*b*) Virtual crack front advance.

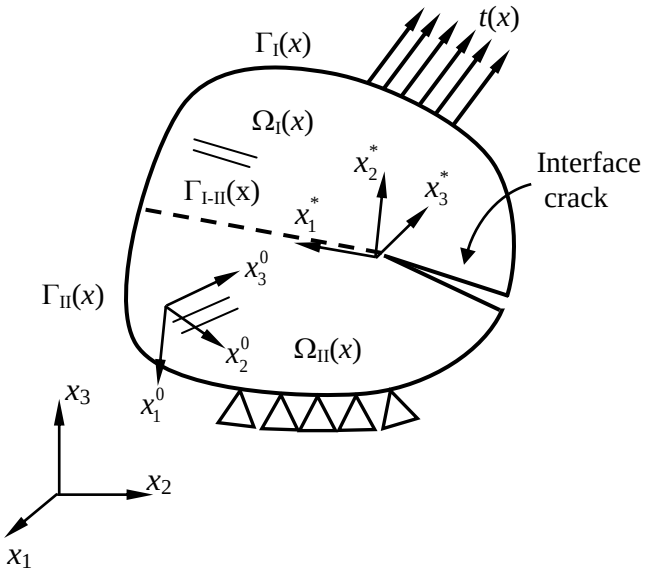

Figure 2: Schematic two-dimensional representation of the multi-domain BEM model with an interface crack.

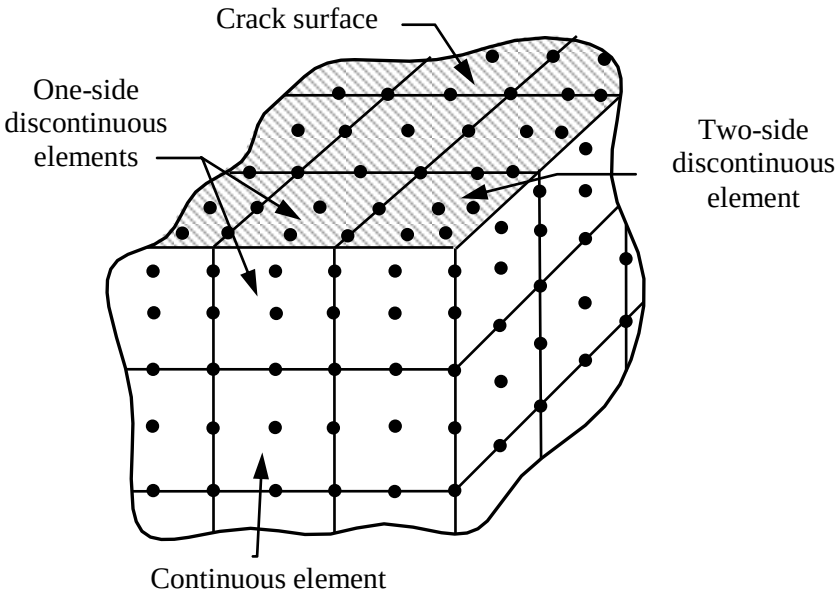

Figure 3: Model discretization strategy using continuous and one- and two-side discontinuous elements.

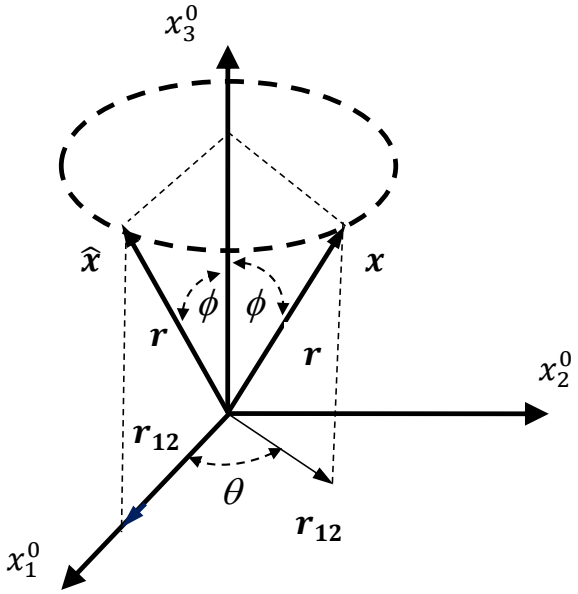

Figure 4: Point **x** and $\hat{\mathbf{x}}$ associated with a transversely isotropic material.

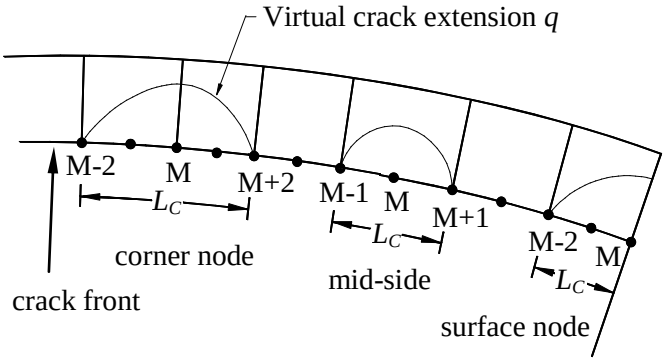

Figure 5: Schematic of the crack front region illustrating the q-function assimilated to the virtual crack extensions for a corner node, a mid-node and a surface node.

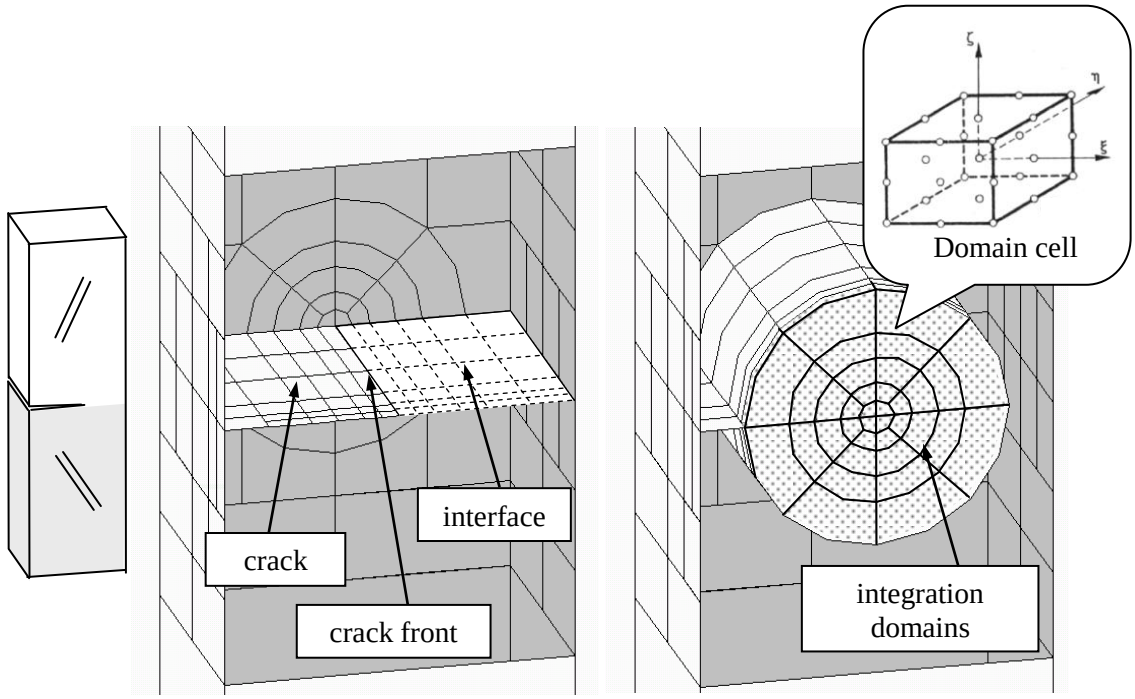

Figure 6: (*a*) Problem geometry, (*b*) Boundary Element discretization, (*c*) Integration domains. Note in figure (c) the detail illustrating the 27-noded isoparametric (brick) cells. The dotted region indicates the volume cells defining the integration volumes used for the computation of the *J*-integral for the crack-front node on the specimen surface (see surface node in Figure 5).

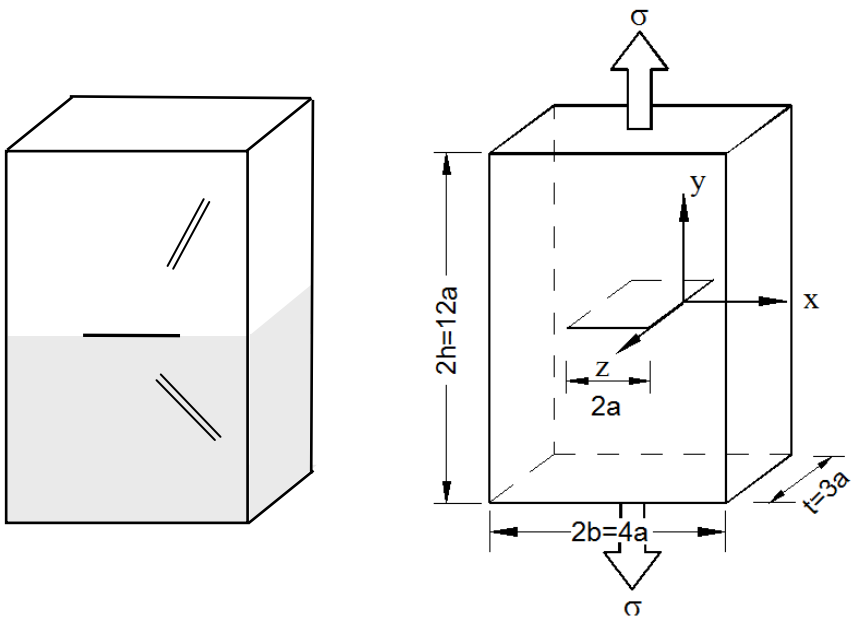

(a) *(b)*

Figure 7: (*a*) Schematic representation of the thick tension plate with a centre interface crack, (*b*) Model dimensions.

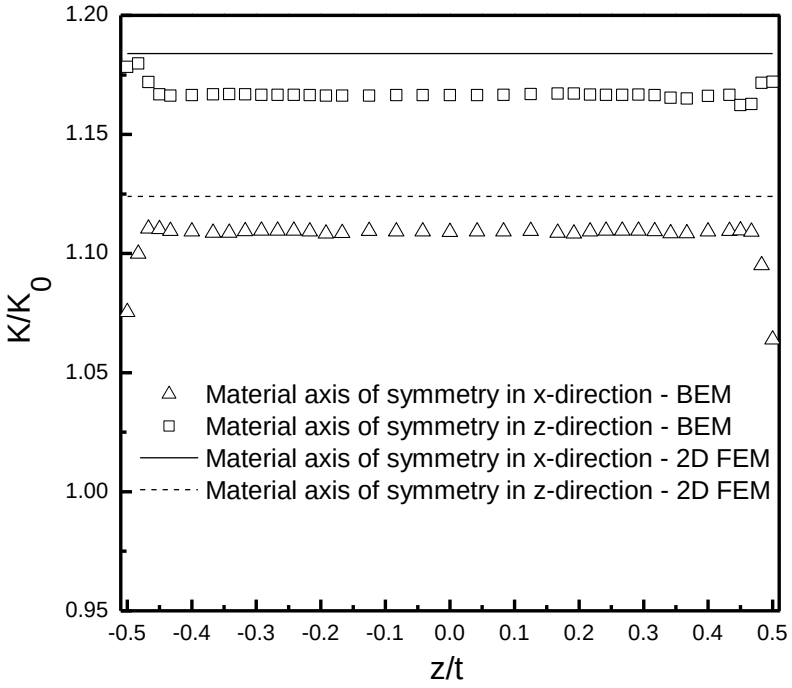

Figure 8: Normalized *SIF* results along the crack front for the homogeneous transversely isotropic centre crack specimen.

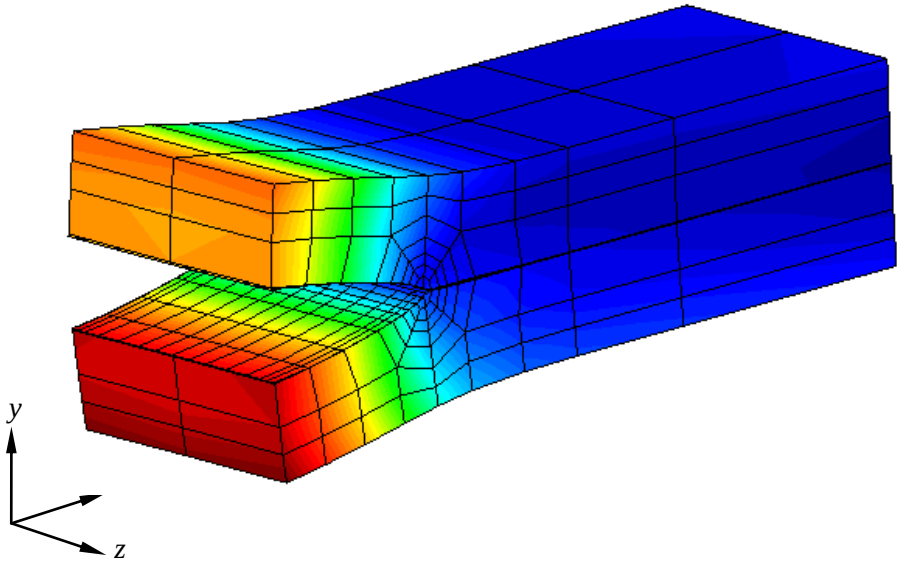

Figure 9: Bimaterial laminate with an edge crack (deformed geometry)

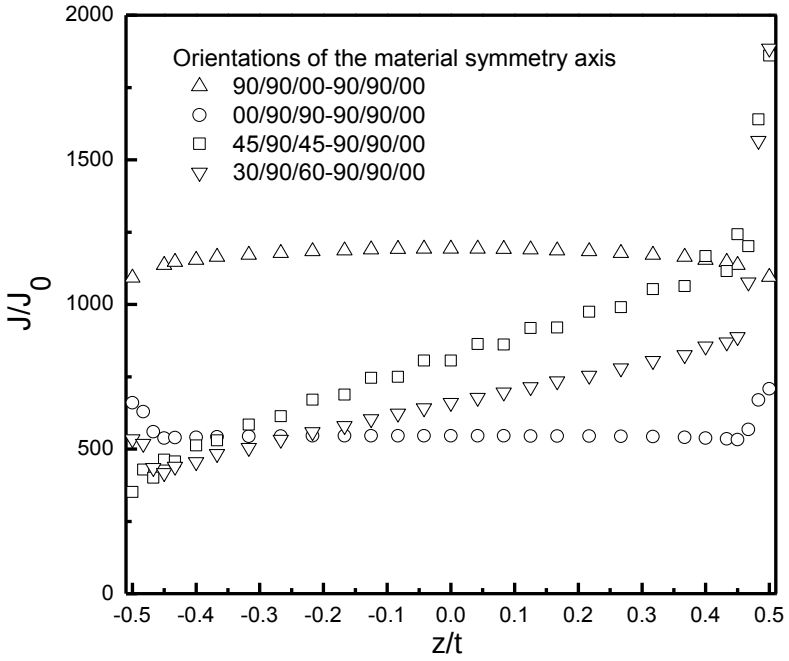

Figure 10: Normalized *J*-integral results along the crack front of the edge crack in the ply.

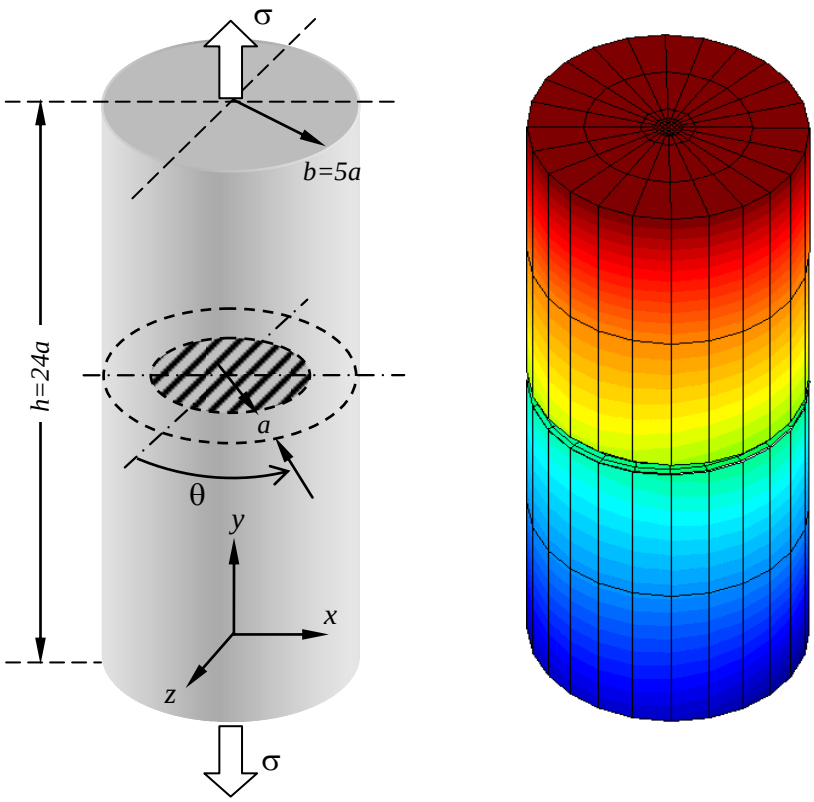

Figure 11: External circumferential interface crack in a cylindrical bimaterial bar, (*a*) model geometry and dimensions, (*b*) model discretization (deformed mesh)

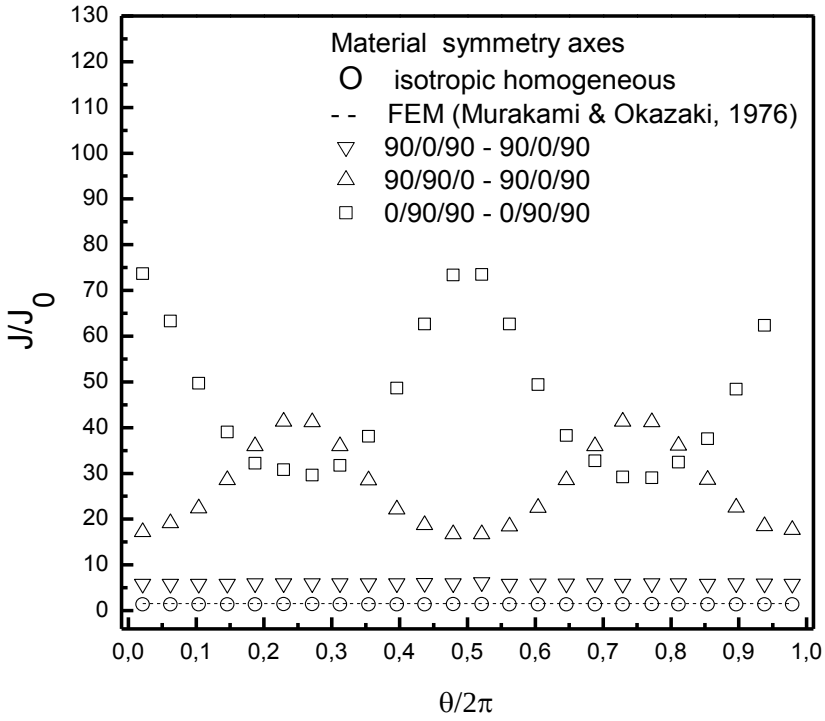

Figure 12: Normalized *J*-integral results along the crack front of the circumferential crack in the biomaterial bar.

Table 1: Values of the coefficients a_{11} and the Young Modulus ratios used in the expression (41)

Case	a_{11}	E_x/E_y
Material symmetry in *x*- direction	$0.112\ 10^{-9}$	49.57
Material symmetry in *z*- direction	$0.2\ 10^{-9}$	1

Table 2: Normalized *J*-integral results for the heterogeneous plate as a function of the integration domain size. The results for the smallest integration domains, *r/a*=0.1 (shaded column in the table) are excluded for the computation of the average value and the STD.

z/t	*r/a*					Average	STD
	0.10	0.20	0.30	0.44	0.64		
0.000	25.6382	30.4503	30.7658	30.7658	30.6081	30.5613	0.49
0.042	25.6382	30.4503	30.7658	30.7658	30.6081	30.5566	0.49
0.083	25.6382	30.4503	30.7658	30.7658	30.6081	30.5512	0.49
0.125	25.6382	30.4503	30.7658	30.7658	30.6081	30.5452	0.49
0.167	25.6382	30.4503	30.7658	30.7658	30.6081	30.5384	0.49
0.192	25.6382	30.4503	30.6869	30.7658	30.6081	30.5306	0.44
0.217	25.6382	30.4503	30.6869	30.7658	30.6081	30.5231	0.44
0.242	25.6382	30.4503	30.6869	30.7658	30.6081	30.5144	0.44
0.267	25.6382	30.4503	30.6869	30.7658	30.6081	30.5041	0.44
0.292	25.6382	30.4503	30.6869	30.7658	30.6081	30.4917	0.44
0.317	25.6382	30.3714	30.6869	30.6869	30.5292	30.4766	0.50
0.342	25.6382	30.3714	30.6081	30.6869	30.4503	30.4651	0.47
0.367	25.6382	30.3714	30.6081	30.6081	30.4503	30.4559	0.39
0.400	25.5593	30.3714	30.6081	30.6081	30.4503	30.4470	0.39
0.433	25.5593	30.2925	30.6081	30.6081	30.4503	30.4345	0.50
0.450	25.5593	30.2925	30.5292	30.6081	30.4503	30.4207	0.44
0.467	25.4804	30.2925	30.6869	30.7658	30.6869	30.4043	0.70
0.483	25.0071	29.9770	30.7658	31.1603	31.2391	30.3024	1.91
0.500	23.5871	28.5570	29.7403	30.3714	30.6081	29.8192	3.08